Enhanced photocatalytic degradation of pure and Cu-doped ZnO nanoparticles prepared under Co-precipitation method

V. Balasubramanian[a], R. Jeyachitra[b], T. S. Senthil[c], S. Kalpana[d,*a]*Department of Physics, Sona College of Technology, Salem – 636005, India*
[b]*Department of Physics, Kalaignar Karunanidhi Institute of Technology, Coimbatore-641402*
[c]*Department of Physics, Erode Sengunthar Engineering College, Perundurai 638057, Tamil Nadu, India*
[d]*Department of Physics, Saveetha Engineering College, Chennai 602105, Tamil Nadu, India*

The key goal of this study is to innovate the pure and 0.05, 0.10 and 0.15 wt.% of Cu-doped ZnO NPs through co-precipitation technique. PXRD pattern shows the hexagonal crystal structure with no any phase impurity were observed for all the synthesized samples. From UV-Vis DRS spectra, band gap was obtained as 3.18, 3.24, 3.29 and 3.33 eV respectively for undoped, Cu-doped ZnO NPs (0.05, 0.10 and 0.15 wt.%). From SEM analysis, the agglomeration of rod-like morphology for pure ZnO NPs, spherical-like morphology for Cu-doped ZnO NPs (0.05 wt.%) and flake-like morphology for Cu-doped ZnO NPs (0.10 wt.%) and flower-like morphology for Cu-doped ZnO NPs (0.15 wt.%). The photocatalytic performance of the synthesized NPs was studied by the dye degradation of Methylene Blue (MB) under UV irradiation. The result exposed that, 0.15 wt.% of Cu-doped ZnO NPs is found to have efficient degradation candidate materials.

(Received September 14, 2023; Accepted February 1, 2024)

Keywords: Cu-doped ZnO NPs, Co-precipitation, Rod-like morphology, Photocatalytic activity, Methylene blue

1. Introduction

Zinc oxide (ZnO) nanoparticles (NPs) is a useful n-type semiconducting material with a direct band gap of 3.37 eV, hexagonal structure, good transparency, high electron mobility (60 meV), high photo stability and non-toxicity, which is used for several applications like photocatalytic activity, opto-electronics, photoconductive, spintronics, sensors, solar cell, batteries, anti-microbial activity and liquid crystal display [1-2]. Several synthesis techniques such as sol–gel technique, combustion technique, sonochemical techniques, polyol techniques, hydrothermal techniques and co-precipitation techniques are used to synthesis the ZnO NPs [3-4]. When compared to other reported techniques, the Co-precipitation technique is the most suitable for the preparation of NPs due to its simplicity, case of mass production, cost-effectiveness, no need for higher pressure and temperature [5]. In current trends, many researches are doping several transition elements (Cu, Cr, Mg, Mn, Ni, Cu, Fe, Cd and Zr) with ZnO NPs could enhanced their unique chemical and physical properties and it has high potential application in many electronic, optoelectronic and spintronics devices [6].

Synthetic dyes in aquatic ecosystems can have adverse effects on marine life and human health. In particular, textile industries are use large quantities of Methylene Blue (MB), a high toxicity dye that can cause several disorders in humans and animals such as convulsions, eye burns, skin irritation, heart palpitations and suffocation. Ingestion may cause gastro intestinal irritation, causing vomiting, cyanosis, diarrhea, and nausea [7]. Based on the high redox potential, durability, biocompatibility, outstanding physical and chemical properties, ZnO has attracted much interest as a useful material for wastewater treatment by photo-catalysis [8]. Unfortunately, the

* Corresponding author: kalpanarajan30@gmail.com
https://doi.org/10.15251/JOR.2024.201.103

high recombination frequency of photo-generated electron-hole pairs, resulting in low quantum output, restricts its use. As a result, much work has gone into improving the photocatalytic performance of ZnO NPs by preventing photo-generated electron-hole pairs from recombination. Doping transition metal ions with ZnO increases the bandgap energy and decreases their charge carrier composition, which increases the photocatalytic efficiency [9]. The enhanced degradation of methylene blue under visible irradiation using Gd-doped ZnO NPs were reported by Saravanan Selvaraj et al., (2019) [10]. The improved photocatalytic activity of Cu-doped ZnO nanoparticles under visible light irradiation were reported by K.G. Kanade et al., (2020) [11]. The enhanced photocatalytic activity of Cu-doped ZnO NPs using methylene blue dye was reported by Prasad N et al. (2017) [12-13]. Hence, an effort has been taken to innovate pure and Cu-doped ZnO NPs (0.05, 0.10 and 0.15 wt.%) using a co-precipitation process to increase photocatalytic activity by taking advantage of the mutually supportive effects of metal ion impurities.

2. Experimental method

2.1. Chemicals

Chemicals involved in the experiment are Zinc (II) chloride dihydrate ($ZnCl_2 \cdot 2H_2O$), Copper (II) chloride dihydrate ($CuCl_2 \cdot 2H_2O$), Methylene Blue (MB), Sodium hydroxide [NaOH], Double Distilled (DD) water and Ethanol [C_2H_5OH] (99% purity).

2.2. Synthesis of undopedZnO NPs

$ZnCl_2 \cdot 2H_2O$ (0.5 M) solution was liquified in DD water (50 ml) under the magnetic stirrer at room temperature for 15 mins. Meanwhile, DD water (20 ml) was taken in another beaker to dissolve the NaOH to make an aqueous solution of NaOH and the solution was added dropwise into the above solution until pH attains 12, since pH plays a significant role in the scale, shape and quality of NPs and the mixture was stirred constantly for 3 hours. After the completion of the reaction, the color of the solution was transforms to white. After that, the black color precipitate was formed and then collected precipitates was filtered using ethanol and DD water. Then, the samples were dried by using hot air oven at 80^oC for few hours and calcination at 350˚C (2 hrs.) in a Muffle furnace.

2.3. Synthesis of Cu doped ZnO NPs

$ZnCl_2 \cdot 2H_2O$ (0.5 M) solution was liquified in DD water (50 ml) under magnetic stirrers. Then, 0.05, 0.10 and 0.15 wt.% of $CuCl_2 \cdot 2H_2O$ were separately added into $ZnCl_2 \cdot 2H_2O$ solutions in three different beakers. The remaining procedures is same as preparation of pure ZnO NPs.

2.4. Photocatalytic experiment

The photocatalytic reduction of MB is carried out using aqueous solution taken at a concentration of 15 mg/L was used to test the photocatalytic behavior of the synthesized of undoped and Cu-doped ZnO NPs (0.05, 0.10 and 0.15 wt.%). To perform the photocatalytic activity, 1 mg of the prepared sample was mixed with 100 ml of MB solution separately to start the dye degradation. Then, the dye reduction is tested for 20 minutes' time intervals by using UV–Visible spectroscopy (Watt Philips TL-D 18 UV lamp) in range of wavelength from 200 to 800 nm. In the reduction process, the reduction of MB to LMB is observed. The following formula was used to quantify the degradation efficacy.

$$\eta = \left(1 - \frac{c}{c_0}\right) \times 100\ (\%)$$

where, C$_o$ and C are indicated solution concentration (t = 0) with irradiation time.

3. Results and discussion

3.1. PXRD analysis

PXRD patterns of pure and 0.05, 0.10 and 0.15 wt. % of Cu-doped ZnO NPs were recorded by using X-ray diffractometer (Bruker) and is presented in Figure 1. The diffraction peaks of all the samples are 31.61°, 34.41°, 36.19°, 47.39°, 56.49°, 62.75°, 66.32°, 67.95° and 69.0° with corresponds planes of (100), (002), (101), (102), (110), (103), (200), (112), and (201), respectively.

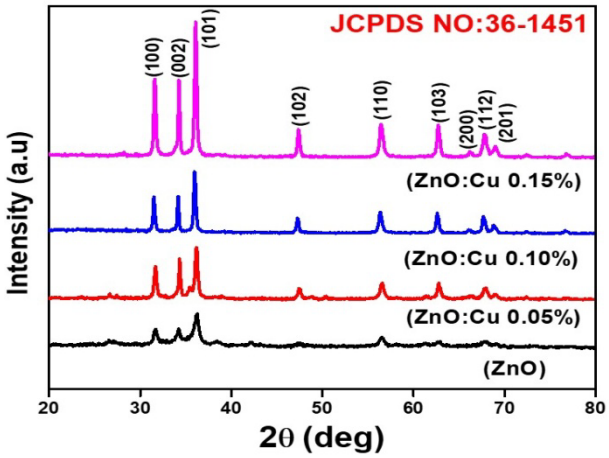

Fig. 1. PXRD patterns of pure and Cu-doped ZnO NPs (0.05, 0.10 and 0.15 wt.%).

The PXRD peaks are well coincide with the hexagonal crystal structure of ZnO NPs (JCPDS card No. 36-1451) [14]. The PXRD patterns expose that there are no extra peaks related to CuO or Cu or Cu_2O which indicated the Cu^{2+} ions were successfully substituted into Zn^{2+} ions in the ZnO lattice without affecting the crystalline nature of the pure ZnO NPs. When compared with undoped ZnO NPs, the observed high diffraction intensity peak (101 plane) of Cu-doped ZnO NPs (0.05, 0.10 and 0.15 wt.%) were increases and shifted towards lower angle side by addition of Cu-dopants due to the intervention of smaller ionic radius of Cu^{2+} (0.073 nm) into larger ionic radii of Zn^{2+} (0.074 nm) are shown in Figure 2 [15-16].

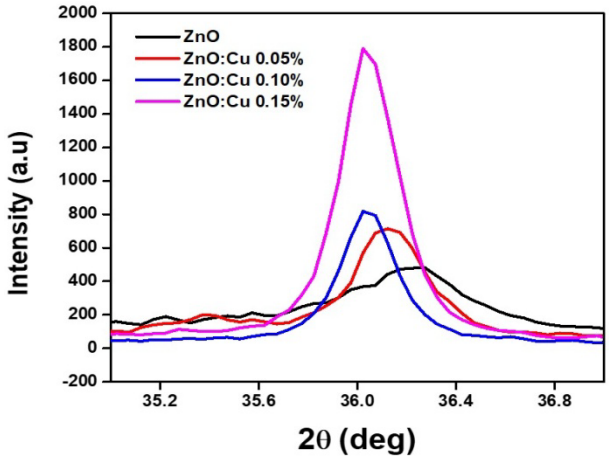

Fig. 2. Magnified PXRD patterns of pure and Cu-doped ZnO NPs (0.05, 0.10 and 0.15 wt.%).

The average crystallite size was calculated from Debye-Scherrer's equation.

$$D = \frac{K\lambda}{\beta cos\theta}$$

where, λ is the X-ray wavelength (0.1541 nm), θ is diffraction angle, D is the particle size, K refers to shape consistency factor (0.9) and β is Full Width Half Maximum (FWHM). The calculated crystallite size values are found to be decreased as 38.46 nm for pure ZnO NPs, 36.26, 33.31 and 29.93 nm for 0.05, 0.010 and 0.15 wt. % Cu-doped ZnO NPs respectively. The average of crystallite size decreases with increasing Cu dopants in ZnO NPs.

3.2. Raman spectroscopy analysis

The measurements of Raman spectroscopy of synthesized samples are performed in the spectral range from 200 to 1000 cm^{-1}. Raman spectrum of pure and Cu-doped ZnO NPs (0.05, 0.10 and 0.15 wt.%) and peaks position at 197 cm^{-1} and 438 cm^{-1} respectively were shown in Figure 3.

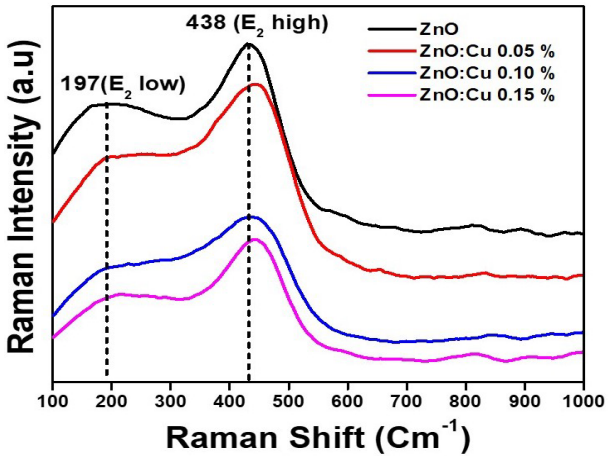

Fig. 3. Raman Spectra of pure and Cu-doped ZnO NPs (0.05, 0.10 and 0.15 wt.%).

From the Raman spectra, the peak at 438 cm^{-1} is observed in pure and Cu-doped ZnO NPs (0.05, 0.10, and 0.15 wt.%) and ascribed to E_2 (high) mode. The high-frequency E_2mode predominantly involves lighter oxygen atoms displacements. The peak at 197 cm^{-1} corresponds to second order nonpolar E_2(low) mode [17-18]. From the figure, the decrease of intensity of E2 (high) mode with increasing Cu doping concentration in ZnO NPs was ascribed to the change in lattice compression happened due to the substitution of smaller ionic radius of Cu^{2+} (0.073 nm) into larger ionic radii of Zn^{2+} (0.074 nm) [17]. The broadening of the E2 peak with the increase of Cu-doping indicates the defects like oxygen vacancies and dislocations in the ZnO NPs. Also, it is can be seen that the concentration of Cu increases from 0.05 to 0.15 wt. % in the ZnO phonon mode at 197 and 438 cm^{-1} is shifted towards higher wavenumber side due to the change in binding energy of the Zn-O bond. As a result of replacing Zn^{2+} by Cu^{2+} and due to the induced strain, phonon confinement by boundaries and force constant changes that occurred by the incorporation of Cu-dopants into ZnO lattice [18].

3.3. UV-Vis-DRS analysis

Optical properties of synthesis samples were recorded by Hitachi UV3010 – diffuse refection spectrophotometer (wavelength from 200 nm to 800 nm). Figure. 4 reveals the UV–DRS absorbance spectra of undoped and Cu-doped ZnO NPs (0.05, 0.10 and 0.15 wt.%).

From the fig, blue shift is observed in Cu-doped ZnO NPs (0.05, 0.10 and 0.15 wt.%) when compared to undoped ZnO NPs respectively. For the undoped ZnO NPs, the absorption band

cut-off at 368 nm and it is shifted to 358, 350 and 343 nm for Cu-doped ZnO NPs (0.05, 0.10 and 0.15 wt.%) respectively, and is due to the addition of dopant (Cu). The following Tauc's relation is used for calculating the band gap (E_g) of undoped and Cu-doped ZnO NPs (0.05, 0.10 and 0.15 wt.%) [19].

$$\alpha h\nu = A(h\nu - E_g)^{1/2}$$

where α is denotes to absorption coefficient, hν is denotes to photon energy, A is mention to proportionality constant. The E_g is found by Tauc's plot was drawn between $h\nu$ and $[F(R)\,h\nu]^2$ and is given in Figure 5.

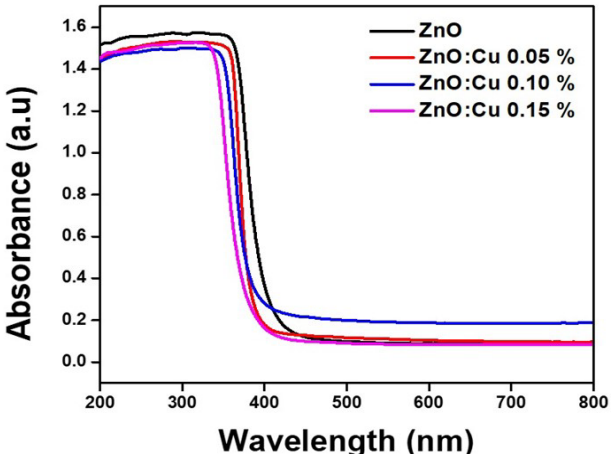

Fig. 4. UV-DRS absorbance spectra of pure and Cu-doped ZnO NPs (0.05, 0.10 and 0.15 wt.%).

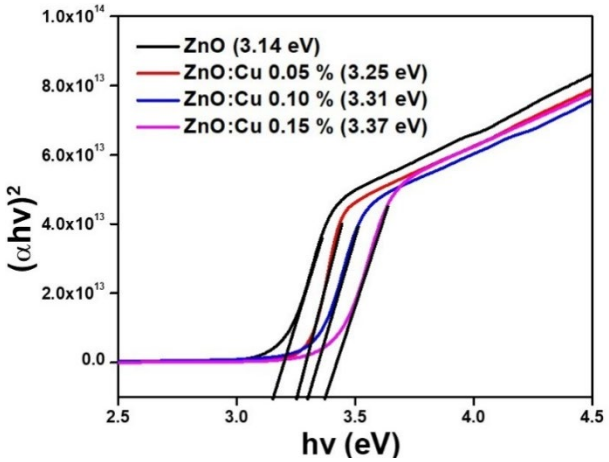

Fig. 5. Tauc's plot of pure and Cu-doped ZnO NPs (0.05, 0.10 and 0.15 wt.%).

The estimated E_g values are 3.14, 3.25, 3.31 and 3.38 eV for pure and Cu-doped ZnO NPs (0.05, 0.10 and 0.15 wt.%) respectively. From the results, the E_g values are decreases with increases in concentration of dopant Cu in ZnO NPs due to various factors mostly existence of quantum confinement effect and oxygen stoichiometry [20]. According to UV reports of the prepared materials, the Cu-doped ZnO NPs (0.15 wt.%) harvested maximum photon energy during the light illumination and which is responsible for enhanced photocatalytic activity, then pure ZnO NPs and Cu-doped ZnO NPs (0.05 and 0.10 wt. %).

3.4. Morphological properties

The morphology of the prepared materials was analysis by SEM along with elemental compositional of dopant in ZnO NPs can be determine by using Energy Dispersive Spectroscopy by using instrument HITACHI S-3400 Scanning Electron Microscopy. SEM images of undoped and Cu-doped (0.05 wt. %, 0.10 wt. %, 0.15 wt. %) ZnO NPs, at the resolution of 1μm and 200 nm are shown in Figure 6 (a-h). Figure 6 (a &b) exposes the agglomeration of rod-like morphology, 6 (c & d) shows the agglomerated spherical-like morphology of Cu-doped ZnO NPs (0.05 wt.%), 6 (e & f) presents the Flake-like morphology of Cu-doped ZnO NPs (0.10 wt.%) and 6 (g&h) shows the Flower-like morphology of Cu-doped ZnO NPs (0.15 wt.%).

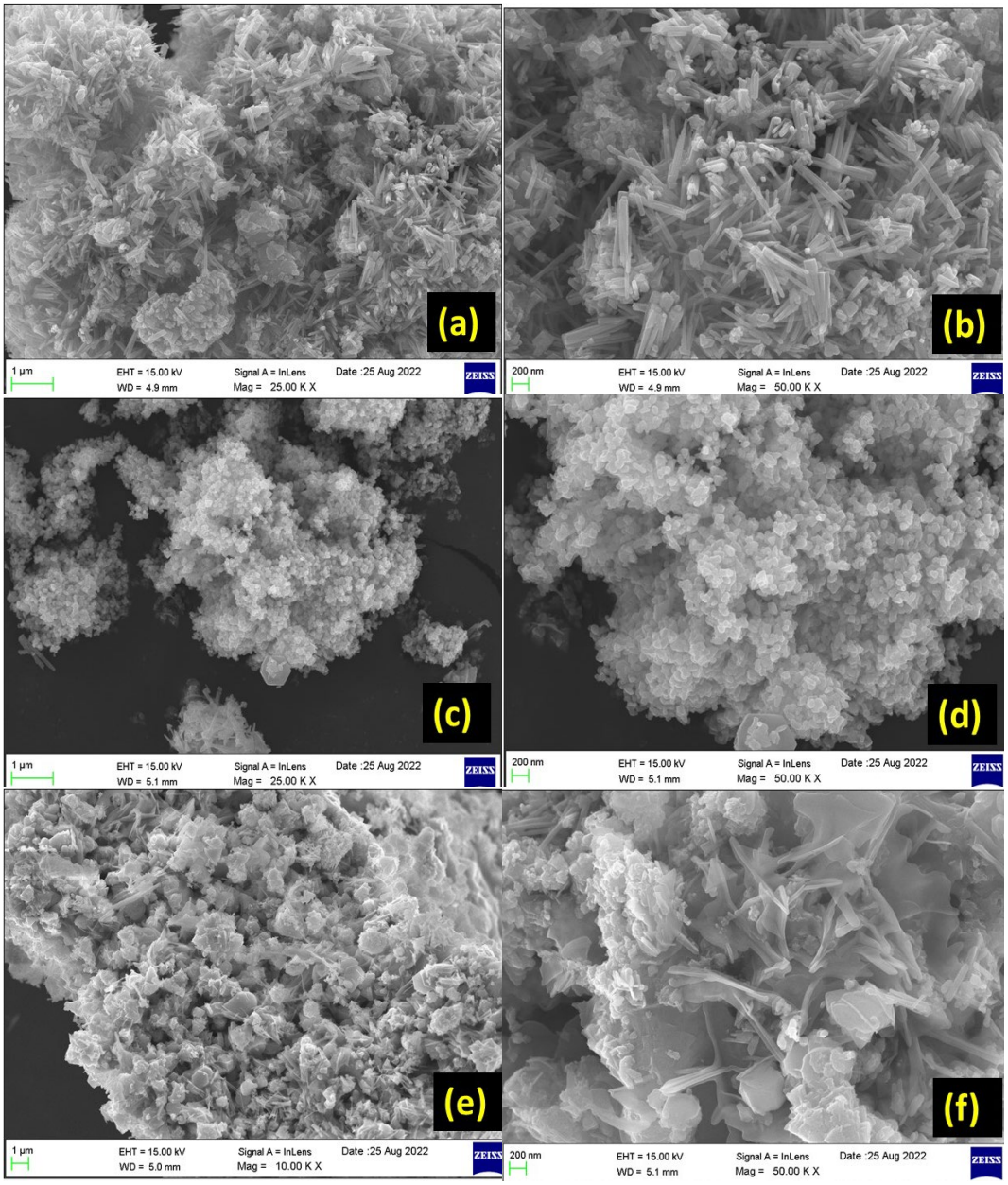

Fig. 6.1.SEM images of (a & b) pure, (c & d) Cu-doped ZnO NPs (0.05wt.%). (e& f) Cu-doped ZnO NPs (0.10 wt.%)

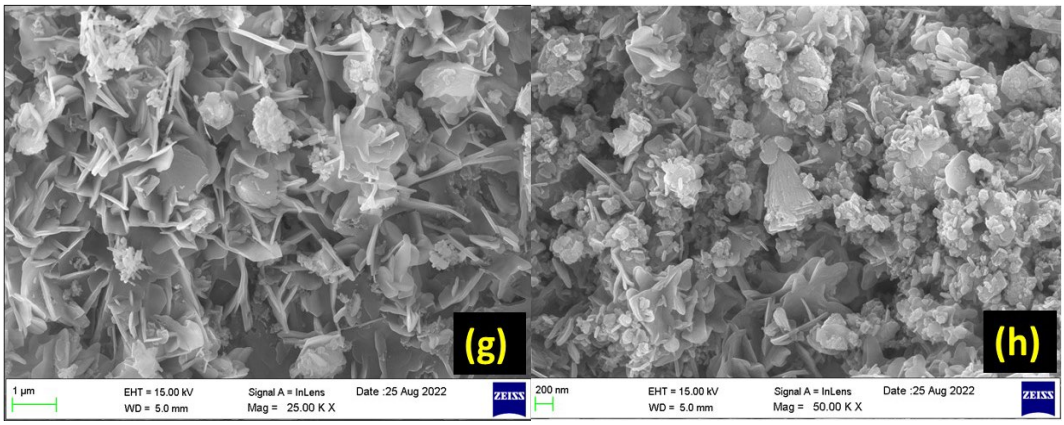

Fig. 6.2.SEM images of (g & h) Cu-doped ZnO NPs (0.15 wt.%).

From the results, it is clear that the morphology of the ZnO is changes due to the agglomeration of the particles and addition of doping elements of Cu.

3.5. Photocatalytic activity

The MB dye degradation by the pure and Cu-doped ZnO NPs (0.05, 0.10 and 0.15 wt.%) in the presence of UV radiation has been studied and is displayed in Figure. 7.

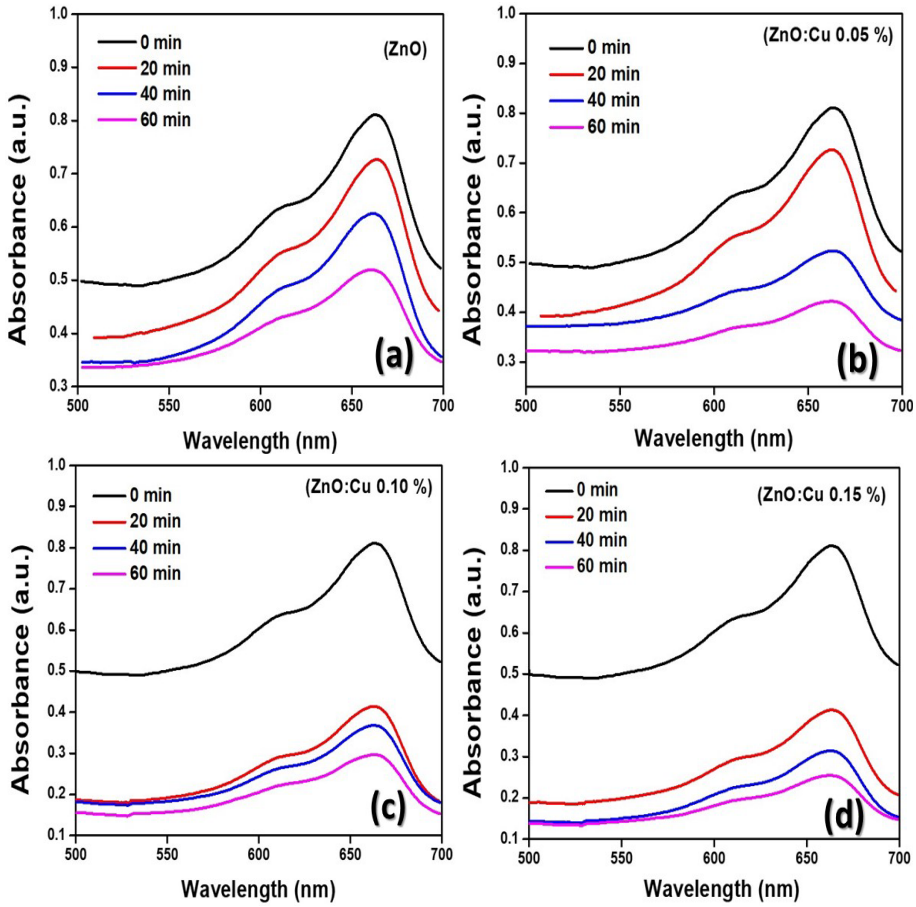

Fig. 7.Time dependent UV absorbance spectra of MB dye with pure and Cu-doped ZnO NPs (0.05, 0.10 and 0.15 wt.%) photocatalysts.

The maximum wavelength (λ_{max}) of MB dye at 664 nm was gradually decreases with intensity which explains that the dye molecules get destructed as the reaction time increases. The corresponding C/C_0 plot against reaction time (T) for MB dye with different photocatalyst is depicted in Figure 8.

The degradation efficiency (%) verses reaction time (T) for pure and Cu-doped ZnO NPs (0.05, 0.10 and 0.15 wt.%) is shown in Figure 9. From the Figure, it is seen that, the degradation efficiency of MB for undoped and Cu-doped ZnO NPs (0.05, 0.10 and 0.15 wt.%) are found to be 43.06 %, 50.37 %, 64.64 % and 72.16 respectively. Also, it confirms the increase of dopant concentration enhances the degradation efficiency. The maximum destruction of MB dye respectively reaches 72.16 % with UV radiation by 0.15 wt.% of Cu-doped ZnO photocatalyst at 60 minutes. From the results, the photon induced recombination of charge carrier is suppressed by addition of Cu^{2+} ions into ZnO NPs, resulting in 0.15 wt. % Cu-doped ZnO NPs degradation efficiency increase.

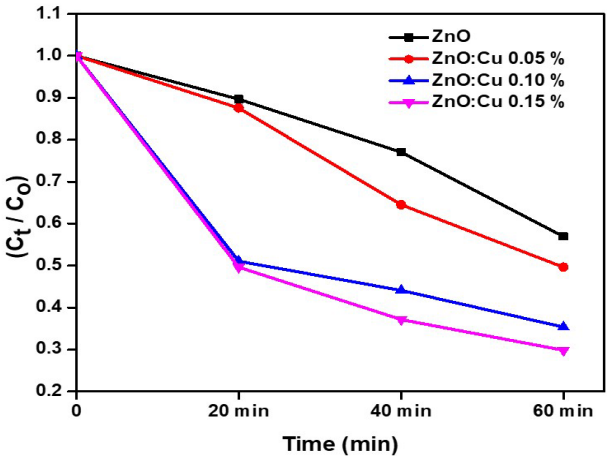

Fig. 8. Variation of C/C_o with reactive time (T) of pure and Cu-doped ZnO NPs (0.05, 0.10 and 0.15 wt.%) for MB dyes.

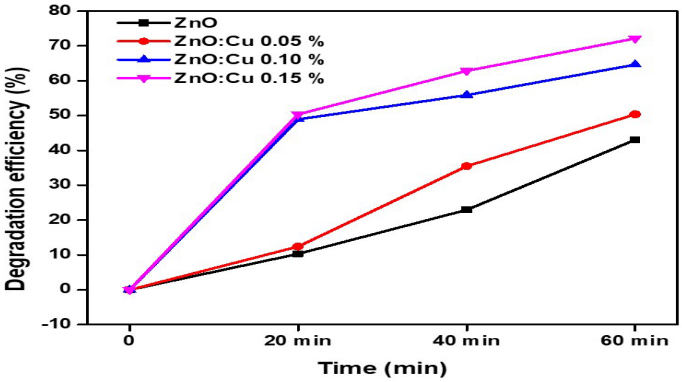

Fig. 9. Variation of degradation efficiency (%) with reactive time (T) of pure and Cu-doped ZnO NPs (0.05, 0.10 and 0.15 wt.%) for MB dyes.

With the simultaneous incorporation of Cu^{2+} impurities, the defect states are created at the conduction band of ZnO with a low energy level resulting in bandgap (3.20 eV), which serves as an electron locking center [21]. The captured electrons then interact with Cu^{2+}, which aids in the degradation of the toxic dye molecule when exposed to UV light. The following is the improved photocatalytic reaction process of 0.15 wt. % Cu-doped ZnO NPs. As light strikes ZnO NPs, the

valence band electrons are triggered and dispersed into the conduction band. The hydroxyl radicals generated by the valence band holes in ZnO then react with water, resulting in dye degradation through the direct oxidation mechanism. By absorbing the ZnO conduction band electrons, the impurity Cu^{2+} ions produce Cu^{2+} ions. The Cu^{2+} ions formed are then transferred an electron into atmospheric oxygen, generating superoxide radicals and Cu^{2+} again. By introducing Cu^{2+} ions into the ZnO crystal structure, the electrons were captured by the defect band, and photo-induced charge carrier coupling was suppressed. As the superoxide radical combines with the water molecule, it releases H_2O_2, which results in the formation of hydroxyl radicals [13]. The hydroxyl radicals created readily interact with dye molecules, which then degrading the synthetic textile contaminants.

3.5.1. Reaction mechanism for the degradation process:

$$[ZnO\ (or)\ Cu{:}\ ZnO] + h\nu \rightarrow h^{+}_{(VB)} + e^{-}_{(CB)}$$
$$Cu^{2+} + e^{-} \rightarrow Cu^{2+}$$
$$Cu^{2+} + O_2 \rightarrow O_2^{\bullet -} + Cu^{2+}$$
$$O_2 + e^{-} \rightarrow O_2^{\bullet -}$$
$$e^{-} + O_2 \rightarrow OH^{-} + OH^{\bullet}$$
$$O_2^{\bullet -} + H_2O \rightarrow HO_2^{\bullet} + OH^{\bullet}$$
$$2HO_2^{\bullet} \rightarrow H_2O_2 + O_2^{\bullet}$$
$$e^{-} + H_2O_2 \rightarrow OH^{-} + OH^{\bullet}$$
$$h^{+} + OH^{-} \rightarrow OH^{\bullet}$$
$$h^{+} + H_2O \rightarrow H^{+} + OH^{\bullet}$$
$$OH^{\bullet} + MB \rightarrow CO_2 + \text{Mineralized products} + H_2O$$
$$O_2^{\bullet -} + MB \rightarrow CO_2 + \text{Mineralized products} + H_2O$$

By evaluating the perceived values of reaction rate constants, the photocatalytic behavior of the synthesized nanomaterials can be quantitatively assessed. The Langmuir-Hinshelwood function governs the photocatalytic decay mechanism and the rate constant (k) is calculated using the equation.

$$ln\left(\frac{C}{C_0}\right) = kt$$

Figure 10 depicts the chart of ln (C/C_0) against irradiation duration of undoped and Cu-doped ZnO NPs (0.05, 0.10 and 0.15 wt.%) respectively for MB dyes.

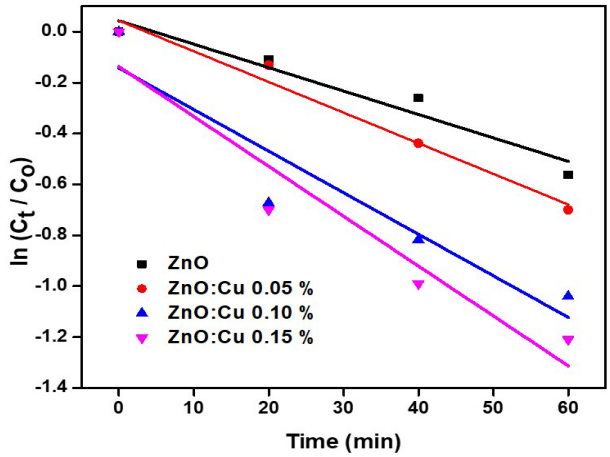

Fig. 10. Variation of ln (C_t/C_o) with reactive time (T) of pure and Cu-doped ZnO NPs (0.05, 0.10 and 0.15 wt.%) for MB dyes.

The observational data and their linear fit are represented by dispersed points and solid lines respectively. The dye degradation mechanism assumes pseudo-first-order reaction kinetics as observed from this graph. The slope of their linear fit lines is used to approximate the reaction rate constant values of undoped and Cu-doped ZnO NPs (0.05, 0.10 and 0.15 wt.%). According to the proportion of this rate constant Cu-doped ZnO NPs (0.15 wt.%) exhibit higher UV photocatalytic behavior than undoped and Cu-doped ZnO NPs (0.05 and 0.10 wt.%) due to the existence of Cu^{2+} ions. The computed rate constant values, R^2 values and percentage of degradation for MB dye with undoped and Cu-doped ZnO NPs (0.05, 0.10 and 0.15 wt.%) photocatalysts are cumulatively tabulated in Table 1.

Table 1.The cumulative photocatalytic result against MB dyes for the prepared materials.

Synthetic Dyes	**Materials**	**Rate constant (k) (s^{-1})**	**(R^2) value**	**Degradation %**
MB	ZnO	13.42×10^{-3}	0.83149	43.06
	ZnO: Cu 0.05 wt. %	14.31×10^{-3}	0.87103	50.37
	ZnO: Cu 0.10 wt. %	16.28×10^{-3}	0.90146	64.64
	ZnO:Cu0.15 wt. %	19.23×10^{-3}	0.92145	72.16

4. Conclusion

In the current investigation to develop pure and Cu-doped ZnO NPs (0.05 and 0.10 wt.%) NPs were synthesized co-precipitation procedure. From the PXRD pattern, it is confirmed that the synthesized all the samples are hexagonal structure without impurity. From the DRS spectra, the addition of dopants increases the energy band gap from 3.14 eV to 3.38 eV due to their quantum confinement effect. Also, the synthesis nanomaterials were used as a photocatalytic activity under UV light irradiation to destroy the MB dye. The Cu-doped ZnO NPs (0.15 wt.%) has revealed maximum degradation efficiency as compared to pure and Cu-doped ZnO NPs (0.05 and 0.10 wt.%) NPs. Under UV light irradiation, the Cu-doped ZnO NPs (0.15 wt.%) achieved 72. 16 % degradation of MB dye (120 minutes). Since, the Cu-doped ZnO NPs (0.15 wt.%) NPs is highly bio-compatible and inexpensive, it may be a good option for photocatalytic dye degradation purposes.

References

[1] N. Senthilkumar, E. Vivek, M. Shankar, M. Meena, M. Vimalan, I. Vetha Potheher, J. Mater. Sci: Mater. Electron. 29, 2927 (2018); https://doi.org/10.1007/s10854-017-8223-5

[2] A. T. Ravichandran, R. Karthick, A. Robert Xavier, R. Chandramohan, Srinivas Mantha, J Mater Sci: Mater Electron. 28, 6643 (2017); https://doi.org/10.1007/s10854-017-6355-2

[3] O.Lupan, G.A. Emelchenko, V.V. Ursaki, G. Chai, A.N. Redkin, A.N. Gruzintsev, I.M Tiginyanu, L. Chow, L.K Ono, B. Roldan Uenya, H. Heinrich, E.E. Yakimov, Mater. Res. Bull. 45, 1026 (2010); https://doi.org/10.1016/j.materresbull.2010.03.027

[4] C. Belkhaoui, N. Mzabi, H.Smaoui, Mater. Res. Bullet. 111, 70 (2029); https://doi.org/10.1016/j.materresbull.2018.11.006

[5] Manish Mittal, Manoj Sharma, O.P. Pandey, Sol. Energy. 110, 386 (2014); https://doi.org/10.1016/j.solener.2014.09.026

[6] K.V. Karthik, A.V. Raghu, Kakarla Raghava Reddy, R. Ravishankar, M. Sangeeta, Nagaraj P. Shetti, Ch Venkata Reddy, Chemosphere 287, 132081 (2022); https://doi.org/10.1016/j.chemosphere.2021.132081

[7] V. Shanmugam, K.S.Jeyaperumal, Applied Surface Science, 449, 617 (2018); https://doi.org/10.1016/j.apsusc.2017.11.167

[8] Darvishi Cheshmeh Soltani, R., Rezaee, A., Khataee, A., Ind. Eng. Chem. Res. 52, 14133 (2013); https://doi.org/10.1021/ie402478p
[9] L. Zheng, C. Chen, Y. Zheng, Y. Zhan, Y. Cao, X. Lin, J. Zhu, Appl. Catal. B. Environ. 148, 44 (2014); https://doi.org/10.1016/j.apcatb.2013.10.042
[10] Saravanan Selvaraj, M. Krishna Mohan, M. Navaneethan, S. Ponnusamy, C. Muthamizhchelvan, Mater. Sci. Semicond. Process. 103, 104622 (2019); https://doi.org/10.1016/j.mssp.2019.104622
[11] K.G. Kanade, B.B. Kale, Jin-Ook Baeg, Sang Mi Lee, Chul Wee Lee, Sang-Jin Moona, Hyunju Chang, Mater. Chem. Phys.102 98 (2007); https://doi.org/10.1016/j.matchemphys.2006.11.012
[12] Prasad N, Karthikeyan B, Vacuum, 146, 501 (2017); https://doi.org/10.1016/j.vacuum.2017.03.028
[13] N. Prasad, V. M. M, Saipavitra, H. Swaminathan, et al., Appl. Phys. A 122, 590 (2016); https://doi.org/10.1007/s00339-016-0121-9
[14] S. Muthukumaran, R. Gopalakrishnan, Optical Materials 34, 1946 (2012); https://doi.org/10.1016/j.optmat.2012.06.004
[15] R. Elilarassi, G. Chandrasekaran, J Mater Sci: Mater Electron. 21, 1168 (2010); https://doi.org/10.1007/s10854-009-0041-y
[16] Talaat M. Hammad, Jamil K. Salem, Roger G. Harrison, Rolf Hempelmann, Nasser K. Hejazy, J Mater Sci: Mater Electron. 24, 2846 (2013); https://doi.org/10.1007/s10854-013-1181-7
[17] T. Srinivasulu, K. Saritha and K.T. Ramakrishna Reddy, Modern Electron. Mater. 3(2), 76 (2017); https://doi.org/10.1016/j.moem.2017.07.001
[18] R Raji, K G Gopchandran, Mater. Res. Express 4, 025002 (2017); https://doi.org/10.1088/2053-1591/aa5762
[19] L. Ben Saad, L. Soltane, F. Sediri, Russ. J. Phys. Chem. 93, 2782 (2019); https://doi.org/10.1134/S0036024419130259
[20] Sabbaghan, Maryam; Nadafan, Marzieh; Lamei, Hamid Reza, Optical Materials, 111, 110679 (2021); https://doi.org/10.1016/j.optmat.2020.110679
[21] P.D. Sahare, V. Kumar, Int. J. Innov. Technol. Explor. Eng. 3, 2278 (2013).